Estimation of robustness of time integration algorithms for elasto-viscoplastic modelling of soils

Zhen-Yu YIN[1], Jian LI[2*], Yin-Fu JIN[3] and Feng-Yin LIU[4]

[1] Associate Professor, Department of Civil and Environmental Engineering, The Hong Kong Polytechnic University, Hung Hom, Kowloon, Hong Kong; Research Institute of Civil Engineering and Mechanics (GeM), UMR CNRS 6183, Ecole Centrale de Nantes, France. Email: zhenyu.yin@gmail.com

[2*] Ph. D., Key Laboratory of Urban Underground Engineering of Ministry of Education, School of Civil Engineering, Beijing Jiaotong Univ., Beijing 100044, China. (corresponding author) Email: jianli@bjtu.edu.cn

[3] Ph. D., Research Institute of Civil Engineering and Mechanics (GeM), UMR CNRS 6183, Ecole Centrale de Nantes, Nantes 44321, France. Email: yinfu.jin9019@gmail.com

[4] Professor, Inst. of Geotechnical Engineering, Xi'an Univ. of Technology, Xi'an 710048, China. Email: liufy@xaut.edu.cn

ABSTRACT: Time integration with stress-strain update is a key step for the application of elasto-viscoplastic models to engineering practice. Currently the estimation of robustness of algorithms is lack which poses difficulties in how to select and improve algorithms. To solve this, the paper selects four typical implicit time integration algorithms, i.e. Newton-Raphson, Katona's, Stolle's and cutting plane algorithms, for a same simple elasto-viscoplastic model EVP-MCC. Some necessary enhancements are discussed and made for the integration. A series of laboratory tests are simulated, based on which the variations of the relative errors of stresses and iteration numbers with step size are investigated and compared. For the Newton-Raphson algorithm and Katona's algorithm with $\theta = 0.5, 1.0$, the maximum step sizes ensuring the convergence have at least one order of magnitude larger than that of other algorithms, and their total iteration numbers and relative errors of stresses have at least one order of magnitude lower than that of other algorithms. Furthermore, the model using different algorithms is implemented into a finite element code, where the global convergence and calculation time are investigated for a boundary value problem. The robustness of all algorithms is estimated based on the calculation performance in terms of convergence, accuracy and efficiency. The results demonstrate that the global iteration number for the cutting plane algorithm is at least 20 times higher than the others at any mesh densities,

which leads to the result that the CPU time for the cutting plane algorithm is almost 10 times higher than the others. All comparisons demonstrate the performance of different time integration algorithms with a prior order of Newton-Raphson, Katona's, Stolle's and cutting plane algorithms.

Keywords: viscoplasticity, implicit integration, finite element analysis, soils, overstress theory

INTRODUCTION

Soils exhibit generally time-dependent stress-strain relationships (e.g., Graham et al. 1983; Leroueil et al. 1985; Nash et al. 1992; Sheahan et al. 1996; Di Prisco et al. 2002; Sorensen et al. 2007; Wang et al. 2008; Wang et al. 2012; Yin et al. 2014, 2017; Yao et al. 2015). The time-dependent nature of soils has a significant impact on geotechnical engineering practice (e.g., Hinchberger and Rowe 2005; Karstunen and Yin 2010; Wang et al. 2011; Yin et al. 2015; Rezania et al. 2016). This effect is normally taken into account in design in elasto-viscoplastic models implemented into finite element codes. In a finite element analysis, the stress increments are computed by the known increments of strain and time for a viscoplastic formulation at each integration point. According to the solution strategy, integration algorithms for an elastoplastic model broadly classified as explicit or implicit. Explicit algorithms are generally coded with automated substepping and error control to maintain the desired accuracy (Sloan et al. 2001). Implicit algorithms, which solve the non-linear constitutive equations by iteration, are generally accurate and unconditionally stable. The attention is made here to implicit time integration schemes only.

In a rate-independent plasticity formulation, the plastic multiplier is calculated by applying the plastic consistency condition on the yield surface. For getting accurate plastic strain increment, a correction loop will iterate until the stress state approximated by the yield surface for implicit stress integration schemes of elastoplastic models. Different from this, the stress state is not always at the static or reference surface in a viscoplastic formulation. Thus, various time integration schemes have been proposed for elasto-viscoplastic models during last decades. For instance, Katona (1984) proposed a one-parameter time integration

algorithm for an elasto-viscoplastic cap model of rocks and soils based on the overstress theory of Perzyna (1963, 1966), wherein a hardening cap surface, a nonhardening failure serface and a tension cutoff criterion are employed. This proposed parameter controls the transformation from explicit to implicit methods or reverses using a Newton-Raphson iterative technique. The Katona's method is widely used for advanced elasto-viscoplastic model, e.g., the cap model under high strain-rate loading by Tong and Tuan (2007), the model considered anisotropy and destructuration by Yin et al. (2010, 2011) and Rezania et al. (2016). Based on a scheme developed by Borja and Lee (1990) for plasticity, Stolle et al. (1999) presented an implicit time-stepping algorithm also for a creep based elasto-viscoplastic cap model of soft soils, wherein the cap surface of modified Cam-Caly model (Roscoe and Burland 1968) was adopted and an accumulated creep strain acted as a strain hardening parameter using a scheme similar to that developed by Borja and Lee (1990) for plasticity. Following the work of Ortiz and Simo (1986), Higgins (2011) applied the cutting plane algorithm for an elasto-viscoplastic model of sand combined with the concepts of the bounding surface plasticity theory and the critical state soil mechanics. Besides of these typical schemes, the Newton-Raphson method was often adopted for the time integration of elasto-viscoplastic models of clays (Yin and Hicher 2008).

However, the numerical performance such as convergence and accuracy has not been comparatively estimated for these implicit time integration schemes. This paper assesses them using a simple elasto-viscoplastic model. Since the model is simple, the convergence and accuracy of algorithms can be highlighted. Four typical numerical algorithms, i.e., Newton-Raphson algorithm, Katona's algorithm, Stolle's algorithm and cutting plane algorithm, are selected and reasonably enhanced for the model. Their performances for an integration stress point are compared by predicting a series of laboratory tests, and the effects of time integration schemes with mesh densities on the global convergences and calculation times are also measured for an undrained plane strain simple shear test in a finite element code.

TIME INTEGRATION ALGORITHMS

Brief Introduction of Simple Elasto-Viscoplastic Model of Soft Clay

The simple elasto-viscoplastic model (EVP-MCC) is a reduced version of ANICREEP model by Yin et al. (2010, 2011) with erasing the anisotropy of reference surface and the destructuration related intrinsic surface. Then the model can be regarded as the combination of Modified Cam-Clay model (Roscoe and Burland 1968) and overstress theory of Perzyna (1963, 1966). The framework of the simple elasto-viscoplastic model is briefly described as follows.

The strain rate $\dot{\boldsymbol{\varepsilon}}$ is assumed to consist of two parts,

$$\dot{\boldsymbol{\varepsilon}} = \dot{\boldsymbol{\varepsilon}}^{e} + \dot{\boldsymbol{\varepsilon}}^{vp} \tag{1}$$

where $\dot{\boldsymbol{\varepsilon}}$ denotes the total strain rate tensor, and the superscripts *e* and *vp* stand, respectively, for the elastic and the viscoplastic components. The elastic behaviour in the proposed model is assumed to be isotropic similarly to the Modified Cam-Clay model. The viscoplastic strain rate is defined by:

$$\dot{\boldsymbol{\varepsilon}}^{vp} = \mu \langle \Phi \rangle \frac{\partial f_d}{\partial \boldsymbol{\sigma}'} \tag{2}$$

where μ is referred to as the fluidity parameter; Φ is the overstress function representing the distance between the dynamic loading surface and the reference surface; f_d is the function of dynamic loading surface corresponding to current effective stress state; $\boldsymbol{\sigma}'$ is the effective stress tensor and is defined by $\boldsymbol{\sigma}' = \boldsymbol{\sigma} - u_w \boldsymbol{\delta}$ with the total stress tensor $\boldsymbol{\sigma}$, the pore water pressure u_w and the Kronecker's delta $\boldsymbol{\delta}$.

In the present model, the overstress function is given by:

$$\Phi = \left(\frac{p_m^d}{p_m^r} \right)^{\beta} \tag{3}$$

where p_m^d and p_m^r represent the sizes of the dynamic loading surface and the reference

surface, respectively (see Fig. 1); β is the strain-rate coefficient. For the practical convenience, the secondary compression coefficient $C_{\alpha e}$ was used as input, and the μ and β were modified as (Yin et al., 2015),

$$\mu = \frac{C_{\alpha e}}{\tau_r (1+e_0)(1-\eta_{K0}^2 / M_c^2)}, \quad \beta = \frac{\lambda - \kappa}{C_{\alpha e}} \tag{4}$$

where e_0 is the initial void ratio; λ is the slope of the normal compression line; κ is the slope of the swelling line; η_{K0} is the stress ratio under the condition of K_0-consolidation with $\eta_{K0} = \left(\sqrt{9+4M_c^2} - 3\right)/2$ according to the stress-dilatancy relationship of the modified Cam-Clay model; M_c is the slope of CSL in the *p'*-*q* (mean stress - deviatoric stress) plane under the condition of triaxial compression; τ_r is the duration of incremental loading used in the conventional oedometer test with a common value of 24 h.

The dynamic loading surface has an ellipsoidal shape (as shown in Fig. 1), and is defined by:

$$f_d = \frac{q^2}{M^2 p'} + p' - p_m^d = 0 \tag{5}$$

where M is the slope of CSL in the *p'*-*q* plane.

The reference surface has the same shape as the dynamic loading surface but different size (as shown in Fig. 1). The increment of the hardening parameter p_m^r for the reference surface is defined by:

$$\mathrm{d}p_m^r = p_m^r \frac{1+e_0}{\lambda - \kappa} \mathrm{d}\varepsilon_v^{vp} \tag{6}$$

where ε_v^{vp} denotes the volumetric viscoplastic strain. For the convenience, the preconsolidation pressure σ_{p0} obtained from oedometer test was used as input. Then the initial size of reference surface can be calculated as,

$$p_{m0}^r = \left[\frac{3(1-K_0)^2}{M_c^2 (1+2K_0)} + \frac{(1+2K_0)}{3} \right] \sigma_{p0} \tag{7}$$

where $K_0 = \left(9 - \sqrt{9+4M_c^2}\right) \Big/ 2\sqrt{9+4M_c^2}$ based on the stress-dilatancy relationship of the modified Cam-Clay model under the condition of K_0-consolidation. Note that theoretically both oedometer and isotropic consolidation tests can be adopted. The μ by Eq.(4) would be modified as $\mu = C_{\alpha e}/\tau_r(1+e_0)$ if the isotropic consolidation test is used (η_{K0}=0) with the initial size of reference surface directly equal to the preconsolidation pressure (K_0=1 in Eq.(7)). However, the preconsolidation pressure is practically determined from conventional oedometer test rather than the isotropic consolidation test, since the latter uses a much higher specimen requiring much more time of consolidation. Besides, K_0 according to the modified Cam-Clay model is less appreciable than the estimation by Jaky's formula, and this problem can be fixed by introducing the inclination of the potential surface such as Yin et al. (2010, 2011).

The slope of critical state line for general stress states can be calculated by:

$$M = M_c \left[\frac{2c^4}{1+c^4+(1-c^4)\sin 3\theta} \right]^{\frac{1}{4}} \tag{8}$$

where $c=M_e/M_c$ with M_c and M_e the slope of CSL in triaxial compression and extension respectively; $-\pi/6 \le \theta = (1/3)\sin^{-1}(-3\sqrt{3}J_3/2J_2^{3/2}) \le \pi/6$ with the second and third invariants of deviator stress tensor, i.e., J_2 and J_3, respectively. For the convenience, c = (3-sinϕ_c)/(3+sinϕ_c) according to Mohr-Coulomb yield criterion was used in this study (ϕ_c = friction angle).

This simple elasto-viscoplastic model is different from those proposed in the literature: using parameters of oedometer test in a more convenient way instead of isotropic consolidation test by Kutter and Sathialingam (1992); eliminating the mechanical instability in models of Vermeer and Neher (1999), Yin et al. (2002), Kelln et al. (2008); correcting the flow rule from contraction to dilation when the soil is on the dry side in models of Vermeer and Neher (1999), Leoni et al. (2008). The proposed model involves parameters of modified Cam-Clay model with only one additional parameter of secondary compression coefficient

$C_{\alpha e}$. The determination methods for all these parameters are summarised in Table 1. Since the $C_{\alpha e}$ can be directly measured from a conventional oedometer test which is also needed for the modified Cam-Clay model, no additional experimental cost is required.

Newton-Raphson Algorithm

In order to appropriate for the numerical method, the stress and strain variables are hereinafter expressed as vectors, i.e., $\boldsymbol{\sigma}' = [\sigma'_x, \sigma'_y, \sigma'_z, \tau_{xy}, \tau_{yz}, \tau_{zx}]^T$ and $\boldsymbol{\varepsilon} = [\varepsilon_x, \varepsilon_y, \varepsilon_z, \gamma_{xy}, \gamma_{yz}, \gamma_{zx}]^T$. With the definitions of stress and strain vectors and the foregoing formulation, a general elasto-viscoplastic constitutive relation can be obtained by:

$$\dot{\boldsymbol{\sigma}}' = \boldsymbol{D}(\dot{\boldsymbol{\varepsilon}} - \dot{\boldsymbol{\varepsilon}}^{vp}) \tag{9}$$

where $\boldsymbol{D}$ is elastic matrix. Based on Eq. (6), the increment rate of hardening parameter could be expressed by:

$$\dot{p}_m^r = p_m^r \frac{1+e_0}{\lambda - \kappa} \dot{\varepsilon}_v^{vp} \tag{10}$$

Integrating Eqs. (9) and (10) over one time step Δt, i.e., from time t_n to t_{n+1}, gives:

$$\Delta\boldsymbol{\sigma}' = \boldsymbol{D}\Delta\boldsymbol{\varepsilon} - \boldsymbol{D}\Delta\boldsymbol{\varepsilon}^{vp} \tag{11}$$

and

$$\Delta p_m^r = \Delta\lambda h \quad \text{with} \quad h = p_m^r \frac{1+e_0}{\lambda - \kappa} \frac{\partial f_d}{\partial p'} \tag{12}$$

where $\Delta\boldsymbol{\sigma}' = \boldsymbol{\sigma}'^{n+1} - \boldsymbol{\sigma}'^{n}$ with $\boldsymbol{\sigma}^n = \boldsymbol{\sigma}(t_n)$; similar definitions hold true for $\Delta\boldsymbol{\varepsilon}$ and Δp_m^r. Combining Eqs. (11) and (12), a group of equations can be obtained as:

$$\boldsymbol{G} = \begin{cases} \boldsymbol{\sigma}'^{n+1} - \boldsymbol{\sigma}'^{tr} + \boldsymbol{D}\Delta\boldsymbol{\varepsilon}^{vp} = 0 \\ p_m^{r,n+1} - p_m^{r,n} - \mu\Phi h = 0 \end{cases} \tag{13}$$

where $\boldsymbol{\sigma}'^{tr} = \boldsymbol{D}\Delta\boldsymbol{\varepsilon}$ is the trial elastic stress tensor. $\boldsymbol{\sigma}'^{n+1}$ and $p_m^{r,n+1}$ could be solved by an iterative procedure with the Newton-Raphson method. The flow chart for the time integration

algorithm of Newton-Raphson is shown in Fig. 2.

Katona's Algorithm

Katona (1984) proposed an algorithm for elasto-viscoplastic models, which uses a step by step time integration scheme. Beginning with Eq. (11), according to a one-parameter time integration scheme, the definition of $\Delta\boldsymbol{\varepsilon}^{vp}$ could be modified by:

$$\Delta\boldsymbol{\varepsilon}^{vp} = \Delta t[(1-\theta)\dot{\boldsymbol{\varepsilon}}^{vp,n} + \theta\dot{\boldsymbol{\varepsilon}}^{vp,n+1}] \tag{14}$$

where θ is integration parameter which is in the range $0 \le \theta \le 1$. When $\theta = 0$, $\Delta\boldsymbol{\varepsilon}^{vp}$ is determined directly by the known value $\dot{\boldsymbol{\varepsilon}}^{vp,n}$ and Δt. It implies that the integration scheme is explicit. Additionally, when $\theta > 0$, $\Delta\boldsymbol{\varepsilon}^{vp}$ is related to the unknown value $\dot{\boldsymbol{\varepsilon}}^{vp,n+1}$ at the end of the time step. It implies that the integration scheme is implicit. The solution of $\Delta\boldsymbol{\varepsilon}^{vp}$ could be obtained by an iterative procedure with the time step. It was indicated that the integration scheme is unconditionally stable for $\theta \ge 0.5$.

Substituting Eq. (14) into Eq. (11) gives:

$$\boldsymbol{P}(\boldsymbol{\sigma}'^{n+1}, \dot{\boldsymbol{\varepsilon}}^{vp,n+1}) = \boldsymbol{q}^{n} \tag{15}$$

where $\boldsymbol{P} = \boldsymbol{D}^{-1}\boldsymbol{\sigma}'^{n+1} + \Delta t\theta\dot{\boldsymbol{\varepsilon}}^{vp,n+1}$ and $\boldsymbol{q}^{n} = \Delta\boldsymbol{\varepsilon} - \Delta t(1-\theta)\dot{\boldsymbol{\varepsilon}}^{vp,n} + \boldsymbol{D}^{-1}\boldsymbol{\sigma}'^{n}$. Then the solutions of $\boldsymbol{\sigma}'^{n+1}$ could be obtained by an iterative procedure with the Newton-Raphson method. The flow chart for the Katona's algorithm is shown in Fig. 3. It should be noted that the Katona's algorithm with $\theta = 1.0$ is the same as the Newton-Raphson algorithm, except that the second derivative of plastic potential to the hardening parameter is not used in the Katona's algorithm.

Stolle's Algorithm

Based on the implicit strategy described by Borja and Lee (1990) for elastoplastic models, Stolle et al. (1999) proposed a time integration algorithm for viscoplasticity. When

199 Δt is known, the initial value of $\Delta\boldsymbol{\varepsilon}_0^{vp}$ is calculated by the initial stress $\boldsymbol{\sigma}_0'$. Then an

200 iteration loop is implied to obtain the accurate solutions of $\Delta\boldsymbol{\varepsilon}^{vp}$ and $\boldsymbol{\sigma}'^{n+1}$. The iteration

201 loop comprises: (a) given $\Delta\boldsymbol{\varepsilon}_0^{vp,i}$, to update $\boldsymbol{\sigma}'$ with Eq. (11); (b) based on the updated $\boldsymbol{\sigma}'$,

202 to calculate $\Delta\boldsymbol{\varepsilon}^{vp,i}$ with Eq. (2); and (c) to update $\Delta\boldsymbol{\varepsilon}_0^{vp,i+1} = \Delta\boldsymbol{\varepsilon}_0^{vp,i} + \delta\Delta\boldsymbol{\varepsilon}_0^{vp}$ by:

203 $$\delta\Delta\boldsymbol{\varepsilon}_0^{vp} = \frac{\Delta\boldsymbol{\varepsilon}^{vp,i} - \Delta\boldsymbol{\varepsilon}_0^{vp,i}}{1 - \dfrac{\partial\Delta\boldsymbol{\varepsilon}^{vp,i}}{\partial\boldsymbol{\sigma}'} : \dfrac{\partial\boldsymbol{\sigma}'}{\partial\Delta\boldsymbol{\varepsilon}_0^{vp,i}}} \tag{16}$$

204 Steps (a) to (c) are repeated until $\left\|\delta\Delta\boldsymbol{\varepsilon}_0^{vp}\right\| < Tol$. Once convergence is achieved, the stress is

205 determined and the hardening parameter is updated. The flow chart for the Stolle's algorithm

206 is shown in Fig. 4.

207 As a key point for the time integration, the criterion condition in the iteration loop is

208 modified in the above illustration. Stolle et al. (1999) chose $\left|\delta\Delta\varepsilon_{v0}^{vp}\right| < Tol$ as criterion

209 condition where ε_v^{vp} is the volumetric viscoplastic strain. That is, this criterion condition did

210 not take into account the deviatoric strain increment. In fact, the norm of deviatoric strain

211 increment vector is much larger than the volumetric viscoplastic strain increment when the

212 stress state is nearby the vertical axis endpoints of the elliptical dynamic loading surface

213 (close to the critical state). Thus, the original criterion condition, $\left|\delta\Delta\varepsilon_{v0}^{vp}\right| < Tol$, will lead to

214 fake convergence.

215 **Cutting Plane Algorithm**

216 Following the work of Ortiz and Simo (1986), and Higgins (2011), the cutting plane

217 algorithm was applied to the EVP-MCC, stated in this section. Because the elastic trial stress

218 is assumed to be constant during the correction loop, the stress and hardening parameter

219 increments with respect to t are defined by:

220 $$\frac{\partial\boldsymbol{\sigma}'}{\partial t} = -\mu\Phi\boldsymbol{D}\frac{\partial f_d}{\partial\boldsymbol{\sigma}'} \tag{17}$$

$$\frac{\partial p_m^r}{\partial t} = \mu \Phi h \tag{18}$$

The change of the function Φ with respect to t is given by:

$$\frac{\partial \Phi}{\partial t} = \frac{\partial \Phi}{\partial \boldsymbol{\sigma}'} \frac{\partial \boldsymbol{\sigma}'}{\partial t} + \frac{\partial \Phi}{\partial p_m^r} \frac{\partial p_m^r}{\partial t} \tag{19}$$

where $\frac{\partial \Phi}{\partial \boldsymbol{\sigma}'} = \Phi \frac{n}{p_m^d} \frac{\partial p_m^d}{\partial \boldsymbol{\sigma}'}$ and $\frac{\partial \Phi}{\partial p_m^r} = -\Phi \frac{n}{p_m^r}$.

Substituting Eqs. (17) and (18) into Eq. (19) gives:

$$\frac{\partial \Phi}{\partial t} = -\frac{\Phi}{\bar{t}} \tag{20}$$

where $\bar{t}$ is the instantaneous time and defined by:

$$\bar{t} = \left[\mu \left(\frac{\partial \Phi}{\partial \boldsymbol{\sigma}'} \boldsymbol{D} \frac{\partial f_d}{\partial \boldsymbol{\sigma}'} - K_p \right) \right]^{-1} \quad \text{with} \quad K_p = \frac{\partial \Phi}{\partial p_m^r} \left(p_m^r \frac{1+e_0}{\lambda - \kappa} \right) \frac{\partial f_d}{\partial p} \tag{21}$$

Solving the differential equation (20) gives:

$$\Delta t^i = \bar{t} \ln \left(\frac{\Phi^i}{\Phi^{i+1}} \right) \tag{22}$$

where $\Delta t^i = t^{i+1} - t^i$ is the time elapsed within an iteration of the correction loop.

The Taylor series of the function Φ^{i+1} gives:

$$\Phi^{i+1} = \Phi^i + \frac{\partial \Phi}{\partial t} (t^{i+1} - t^i) \tag{23}$$

Substituting Eq. (20) into Eq. (23) and setting $\Phi^{i+1} = 0$ gives:

$$\Delta t^i = \bar{t}^i \tag{24}$$

According to the expression of strain rate, i.e., Eq. (2), the change in plastic multiplier $\Delta\lambda$ in one iteration of the viscous correction loop is calculated as

$$\Delta\lambda = \dot{\lambda}\Delta t = \mu \Phi \Delta t \tag{25}$$

Then substituting Eqs. (21) and (24) into Eq. (25) obtains:

$$\Delta\lambda = \mu \Phi \Delta t = \mu \Phi \bar{t} = \frac{\Phi}{\frac{\partial \Phi}{\partial \boldsymbol{\sigma}'} \boldsymbol{D} \frac{\partial f_d}{\partial \boldsymbol{\sigma}'} - K_p} \tag{26}$$

The expression of $\Delta\lambda$ is different from that stated by Higgins (2011) due to the overstress function. Then the stress and the hardening parameter can be updated. The flow chart for the cutting plane algorithm is shown in Fig. 5.

According to Eqs. (24) and (26), the change of viscoplastic strain in one iteration is calculated by an instantaneous time in the cutting plane algorithm. The instantaneous time is equal to the time increment in one iteration when $\Phi^{i+1} = 0$ is assumed. This assumption assures the stress could relax to zero when the time is sufficient. In general, however, the stress relaxation would be terminated in a given time increment, which means that the assumption $\Phi^{i+1} = 0$ is not appropriate into the majority situation. Therefore, the iteration number of cutting plane algorithm is much larger than the other three implicit algorithms for a given time step, which will be confirmed by the next section.

Summary of Algorithms

According to the time integration methods, these implicit algorithms can be classified into two categories. In the first category, the viscoplastic strain is directly calculated by the actual time increment and a correction loop will iterate to get the accurate plastic strain increment. In the second category, the viscoplastic strain is calculated by an instantaneous time increment which is obtained according to the corrected and updated values of the stress state and hardening parameter during one correction step. When the difference between the accumulated time increment and the actual time increment is lower than the tolerance value, the accurate solutions are obtained. The time integration algorithms of the Newton-Raphson, Katona (1984) and Stolle et al. (1999) belong to the first category, and the cutting plane algorithm belongs to the second category.

Each kind of time integration method has its own particular characteristics. In the first category of time integration algorithm, the second derivatives of the plastic potential are required. It is noted that the needed second derivatives for the Newton-Raphson algorithm, i.e., the Jacobian matrix $\boldsymbol{J} = \partial \boldsymbol{G} / \partial \boldsymbol{x}$, is more complicated than the others two algorithms in the first category. The Katona's algorithm with $\theta = 1.0$ is the same as the Newton-Raphson algorithm, except that the second derivative of plastic potential to the hardening parameter is not used in the Katona's algorithm. In general, the task of evaluating the second derivatives may prove exceedingly laborious and is best avoided. For the second category of time integration algorithm, i.e., the cutting plane algorithm, it is formulated solely on the basis of the yield function, the normal to the yield surface, the direction of plastic flow and the tangent elastic moduli without their gradients, which is observably different from the above algorithms and is simpler than the algorithms in the first category. However, its convergence speed for a viscoplastic modelling should be doubtful as stated above. Therefore, the robustness of the four algorithms should be discussed for further selection and improvement.

NUMERICAL VALIDATION AT INTEGRATION POINT LEVEL

Integration Scheme for EVP-MCC

To compare the convergence and accuracy of the above time integration algorithms, a step-changed oedometer test and a step-changed undrained triaxial test in compression were simulated using the model with different algorithms. The model parameters are based on a series of laboratory tests on Saint-Herblain clay by Yin et al. (2010), summarised in Table 2. For the step-changed oedometer test, the initial vertical and radial stresses are 10 kPa and 4.9 kPa, respectively. The specimen was consolidated to axial strains of 12 %, 15.5 % and 25 % in sequence with strain rates of 0.02 %/h, 0.004 %/h and 0.02 %/h, respectively. For the step-changed undrained triaxial test, the initial stress state of the specimen is the same as that of oedometer test. The specimen was firstly consolidated to the vertical stress of 86 kPa and the radial stress of 77 kPa in 1 day. Then the specimen was sheared to axial strains of 2%, 2.5%, 4.7% and 6.3% in sequence with strain rates of 1 %/h, 0.1 %/h, 10 %/h and 0.1 %/h,

respectively. Furthermore, a numerical undrained triaxial test in extension was simulated. The initial stress state and the consolidation stage are the same as that of the undrained triaxial test in compression, and its variation of axial strain is inverse but with the same strain rates in shearing stage.

During simulations, different stepsize of strain increments per step is in the range of 10^{-6} to 10^{-2} for oedometer test and 10^{-6} to 5×10^{-3} for undrained triaxial tests. To get the relative errors of calculated results, an ‘‘exact’’ solution is required against which all the approximate solutions can be compared. Such a solution is assumed by each stress integration method with the small step size of 10^{-6}. The relative error of stresses is computed by:

$$E = \sqrt{\frac{1}{N}\sum_{i=1,}^{N}\left(\frac{\sqrt{p_i'^2+q_i^2}-\sqrt{(p_i'^{ex})^2+(q_i^{ex})^2}}{\sqrt{(p_i'^{ex})^2+(q_i^{ex})^2}}\right)^2} \tag{27}$$

where p'^{ex} and q^{ex} are the “exact’’ solutions; N represents the number of compared stress points.

Simulation of Oedometer Test

The comparisons between simulations using different incremental steps and time integration methods for the step-changed one-dimensional oedometer test are given in Figs. 6 and 7. As shown in Fig. 6, the convergences for the Newton-Raphson algorithm and Katona’s algorithm with $\theta = 0.5, 1.0$ are better than the others. The Katona’s algorithm with $\theta = 0$ and Stolle’s algorithm are not convergences when the step size greater than 0.1%, and the cutting plane algorithm is not convergences when the step size greater than 0.25%. Fig. 7 shows that the total iteration number decreases and the relative error of stresses defined by Eq. (27) increases with the increase of the step size. The relative error of stresses for the Katona’s algorithm with $\theta = 0.5$ increases more rapidly than the Newton-Raphson algorithm and Katona’s algorithm $\theta = 1.0$ with the increase of step size. Besides, the total iteration number and the relative error of stresses for the cutting plane algorithm have one order of magnitude higher than the others. Finally, the relative error of stresses for the Newton-Raphson algorithm and Katona’s algorithm with $\theta = 1.0$ is almost the same in the studied range of

316 step size. However, the iteration number for the Newton-Raphson algorithm is lower than that
317 of the Katona's algorithm with $\theta = 1.0$.

318 **Simulation of Undrained Triaxial Tests**

319 The comparisons between simulations using different incremental steps and time
320 integration methods for step-changed undrained triaxial tests in compression and extension
321 are shown in Figs. 8 and 9. As shown in Fig. 8, the convergence of the Newton-Raphson
322 algorithm, Katona's algorithm with $\theta = 0.5, 1.0$ and the cutting plane algorithm is better
323 than the others. As shown in Figs. 8(c) and 8(d), the convergence of the Katona's algorithm
324 with $\theta = 0.0$ is not acceptable. The simulations for the Katona's algorithm with $\theta = 0.0$
325 cannot converge when the step size greater than or equal to 0.025%. Besides, the simulations
326 using the Stolle's algorithm with the step sizes of 0.25 and 0.5 are not illustrated in the Figs.
327 8(i) and 8(j) due to the fact that the calculation results are not convergent.

328 Figs. 9(a) and 9(c) show that the total iteration number decreases with the increase of the
329 step size for all the time integration algorithms except to the Katona's algorithm with $\theta = 0.5$.
330 As shown in Figs. 9(b) and 9(d), the relative error of stresses for the Katona's algorithm with
331 $\theta = 0.5$ and cutting plane algorithm has at least one order of magnitude higher than the
332 others at the studied range of step size. Besides, the variations of relative errors of stresses
333 with step size are not monotonous for the Newton-Raphson algorithm and Katona's algorithm
334 with $\theta = 0.5, 1.0$. Finally, the relative error of stresses for the Newton-Raphson algorithm
335 and Katona's algorithm with $\theta = 1.0$ is almost the same, and the iteration number for the
336 Newton-Raphson algorithm is lower than that of the Katona's algorithm with $\theta = 1.0$,
337 which is the same as what found in simulating oedometer test.

338 # NUMERICAL VALIDATION AT FINITE ELEMENT LEVEL

339 **Model Implementation Scheme into Finite Element Code**

340 A User Defined Soil Model (UDSM) for the elasto-viscoplastic model EVP-MCC has
341 been developed using different time integration algorithms for its usage within the
342 commercial finite element code PLAXIS 2D. The model was programmed following the

rules of the PLAXIS program for implementing user-defined constitutive models as stated in the PLAXIS material models manual (PLAXIS, 2012).

Simulation of Undrained Plane Strain Simple Shear Test

A numerical undrained plane strain test was simulated using PLAXIS to compare global iteration number and global calculation time for different mesh densities by the model with different time integration methods. Model parameters and initial state variables are the same as that used in previous numerical validations at integration point level.

The simulation of undrained plane strain test is briefly introduced as follows. The fully undrained analysis was selected and then the coupled consolidation analysis is not needed. In PLAXIS it is possible to specify undrained behaviour in an effective stress analysis. Pore pressure σ_w includes steady pore pressure p_{steady} and excess pore pressure p_{excess}, in which p_{steady} is just generated data according to the depth of water. Then,

$$\dot{\sigma}_w = \dot{p}_{excess} \tag{28}$$

Considering slight compressibility of water, the pore pressure rate can be expressed as:

$$\dot{\sigma}_w = \frac{K_w}{n}\left(\dot{\varepsilon}_x^e + \dot{\varepsilon}_y^e + \dot{\varepsilon}_z^e\right) \tag{29}$$

where K_w is the bulk modulus of water, and n is the porosity of the soil.

Then, the elastic constitutive relation can be expressed by using the total stress increment with the undrained Young's modulus E_u and the undrained Poisson's ratio υ_u,

$$E_{\mathrm{u}} = 2G\left(1+\upsilon_{\mathrm{u}}\right) = \frac{\upsilon' + \mu\left(1+\upsilon'\right)}{1+2\mu\left(1+\upsilon'\right)} \tag{30}$$

with

$$\mu = \frac{1}{3n}\frac{K_{\mathrm{w}}}{K'},\quad K' = \frac{E'}{3\left(1-2\upsilon'\right)} \tag{31}$$

$$K' = \frac{1+e_0}{\kappa}p',\quad E' = 3K'\left(1-2\upsilon'\right) \tag{32}$$

where E' and υ' are Young's modulus and undrained Poisson's ratio, respectively. Thus, according to previous equations, the option for undrained behaviour in PLAXIS is such tat the effective parameters E' and υ' are replaced by the undrained parameters E_u and υ_u. The detail introduction of undrained effective stress analysis can be referred to PLAXIS material models manual (PLAXIS, 2012).

In the undrained plane strain test, the size of the sample is 0.5 m long and 0.3 m high. The bottom boundary displacement is restrained in the vertical direction. The element type is a 6-noded triangular element. Fine, middle and coarse mesh densities of finite element mesh were chosen to test the mesh dependency, and the corresponding numbers of elements are 552, 270 and 110, respectively. The simulation was conducted in three stages. The sample was firstly isotropically consolidated to a target stress of 1 kPa instantaneously. Then it was K_0-consolidated to an axial displacement increment of 0.02 m with a strain rate of 13.3 %/h. Finally, the bottom boundary displacement was restrained in both vertical and horizontal directions, and the top side of the sample was sheared to a horizontal displacement increment of 0.1 m with the same strain rate of 2.0 %/h.

The comparisons of a total number of iteration and CPU time for different mesh densities by the model with different time integration methods are summarised in Table 3. The global iteration number for the cutting plane algorithm is obviously higher than the others at any mesh density. It leads to the result that the CPU time for the cutting plane algorithm is also higher than the others. Besides, the global iteration number decreases with the decreasing of mesh densities for the cutting plane algorithm. However, the difference of the variation of the global iteration number with mesh densities is slight for others algorithms. Finally, the CPU time decreases with the decreasing of mesh densities for all the time integration algorithms.

The simulated test result of the Newton-Raphson algorithm is illustrated in Fig 10 (a), which shows that the effect of mesh density for the curve of $\sigma_{12} - \gamma_{12}$ is slight. The simulated results for fine, middle and coarse mesh densities by the model with different time

integration methods are shown in Figs 10(b), 10(c) and 10(d), respectively. The simulated curves of $\sigma_{12} - \gamma_{12}$ for the cutting plane algorithm are slightly lower than the others for all the mesh densities.

The shear strain field for fine, middle and coarse mesh densities by the model with the Newton-Raphson algorithm are shown in Figs 11(a), 11(b) and 11(c), respectively. The strain concentration at the corners of the top side is most obvious for the fine mesh density. Besides, the shear strain field for the fine mesh density by the model with the cutting plane algorithm is shown in Fig 11(d). All shear strain fields by different integration methods are similar.

DISCUSSION

Based on the above analysis, the comparisons of the performance of different time integration algorithms are summarised in Table 4. At integration point level, the convergence and accuracy of the Newton-Raphson algorithm and Katona's algorithm with $\theta = 1.0$ are good. It leads to the results that the performance of the two integration algorithms is also good at the finite element level. The convergences or accuracies for the Katona's algorithm with $\theta = 0.5$, Stolle's algorithm and cutting plane algorithm are worse than the above two algorithms at the range of bigger step size. However, it doesn't affect their performance at the finite element level. For the triaxial test in extension, the convergence and accuracy of the Katona's algorithm with $\theta = 0.0$ are poorest at the studied range. It leads to the fail of convergence at the finite element level.

Based on the algorithm introductions of viscoplastic formulation, it is easy to found that the Katona's algorithm with $\theta = 1.0$ is the same as the Newton-Raphson algorithm, except that the second derivative of plastic potential to the hardening parameter is not used in the Katona's algorithm. The convergence speed for obtaining an accurate solution is improved by the additional second derivative of plastic potential in the Newton-Raphson algorithm, and the improvement is gradually obvious with the increase of the step size for different test paths, as shown in Figs 7(a), 9(a) and 9(c). However, there is no difference in their accuracies as shown in Figs 7(b), 9(b) and 9(d), which is mainly attributed to adopted criterion conditions

for iteration loop.

CONCLUSIONS

Four typical implicit numerical algorithms, i.e., Newton-Raphson algorithm, Katona's algorithm, Stolle's algorithm and cutting plane algorithm, are applied to the simple elasto-viscoplastic model, in which the Stolle's algorithm is enhanced by taking into account the deviatoric strain in the criterion conditions for iteration loop. These implicit algorithms can be classified into two categories according to the time integration methods. The viscoplastic strain is calculated by the actual time increment and the instantaneous time increment, respectively, in the two kinds of algorithms. In the first category, the second derivatives of the plastic potential are required which is laborious and is best avoided. In the second category, i.e., the cutting plane algorithm, the instantaneous time is assumed to be equal to the time increment with the condition $\Phi^{i+1}=0$ which would lead to the decreasing of convergence speed.

At the integration point level, the step-changed oedometer test and the step-changed undrained triaxial tests were selected to compare the convergence and accuracy of the above time integration algorithms. Firstly, the maximum step sizes ensuring the convergence of the Katona's algorithm with $\theta=0$ and Stolle's algorithm have at least one order of magnitude lower than that of other algorithms. Especially, the Katona's algorithm with $\theta=0$ is not convergence when the step size greater than 0.01 for undrained triaxial tests. Secondly, the total iteration number and the relative error of stresses of the cutting plane algorithm have at least one order of magnitude higher than that of other algorithms, except that the relative error of stresses of the Katona's algorithm with $\theta=0.5$ is higher than that of the cutting plane algorithm for undrained triaxial tests. Overall, The convergences and accuracy for the Newton-Raphson algorithm and Katona's algorithm with $\theta=0.5,1.0$ are obviously better than the others.

At the finite element level, a numerical undrained plane strain simple shear test was simulated using PLAXIS in which the model using different algorithms was implemented.

Global iteration number and global calculation time for different mesh densities were then compared. Firstly, the global iteration number for the Newton-Raphson algorithm, Katona's algorithm with $\theta = 0.5, 1.0$ and Stolle's algorithm are similar, and its variation with mesh densities is not obvious. However, the CPU time for the Stolle's algorithm is about half of that of the others. Secondly, the global iteration numbers of the fine and middle mesh densities are almost 2 times larger than that of coarse mesh density for the cutting plane algorithm. Besides, the global iteration number for the cutting plane algorithm is at least 20 times higher than that of the others at any mesh densities. As a result, the CPU time for the cutting plane algorithm is almost 10 times higher than the others. Thirdly, the CPU time almost linearly decreases with the decreasing of mesh densities for all the algorithms. Fourthly, the calculation for the Katona's algorithm with $\theta = 0.0$ cannot converge which is consistent with the problem found in the calculation of undrained triaxial test path at the integration point level.

The above comparisons comprehensively illustrate the performances of the different time integration schemes for the EVP-MMC based on the calculation results at both the integration point level and finite element level. The Newton-Raphson algorithm and Katona's algorithm with $\theta = 1.0$ have a better robustness and accuracy than the others, although the obtaining of second derivatives of the plastic potential is unavoidable in the above two algorithms, which increases the difficulty of numerical implementation. Then, the Newton-Raphson algorithm and Katona's algorithm with $\theta = 1.0$ are recommended, since the robustness and accuracy are most important in modelling. Besides, the cutting plane algorithm without needing second derivatives of the plastic potential is optional. However, how to numerically implement a viscoplastic model using this method with good robustness and accuracy remains an issue.

The study is helpful to select and further improve algorithms for developing and implementing advanced elasto-viscoplastic models for geotechnical applications.

ACKNOWLEDGMENTS

We acknowledge with gratitude the financial support provided by the National Natural Science Foundation of China (Grant Nos. 41372285, 51579179, 51608033), and the Region Pays de la Loire of France (project RI-ADAPTCLIM).

REFERENCES

Borja, R. I. and Lee, S. R. (1990). "Cam-clay plasticity, part 1: implicit integration of elasto-plastic constitutive relations." *Comput. Methods Appl. Mech. Engrg.*, 78(1), 49-72.

Di Prisco, C., Imposimato, S., and Aifantis, E. C. (2002). "A visco-plastic constitutive model for granular soils modified according to non-local and gradient approaches." *Int. J. Numer. Anal. Meth. Geomech.*, 26(2), 121-138.

Graham, J., Crooks, J. H. A., and Bell, A. L. (1983). "Time effects on the stress-strain behaviour of natural soft clays." *Géotechnique*, 33(3), 327-340.

Karstunen, M. and Yin, Z.-Y. (2010). "Modelling time-dependent behaviour of Murro test embankment." *Géotechnique*, 60(10), 735-749.

Katona, M. G. (1984). "Evaluation of viscoplastic cap model." *J. Geotech. Engrg.*, ASCE, 110(8): 1106-1125.

Kutter, B. L. and Sathialingam, N. (1992). "Elastic-viscoplastic modelling of the rate-dependent behaviour of clays." *Géotechnique*, 42(3), 427-441.

Higgins, W. T. I. V. (2001). "Development of a High Strain-Rate Constitutive Model for Sands and its Application in Finite Element Analysis of Tunnels Subjected to Blast." Master's thesis, University of Connecticut, Storrs, United States.

Hinchberger, S. D. and Rowe, R. K. (2005). "Evaluation of the predictive ability of two elastic-viscoplastic constitutive models." *Can. Geotech. J.*, 42(6), 1675-1694.

497 Kelln, C., Sharma, J., Hughes, D., and Graham, J. “Finite element analysis of an embankment
498 on a soft estuarine deposit using an elastic-viscoplastic soil model.” *Can. Geotech. J.*,
499 2008, 46(3), 357-368.

500 Leroueil, S., Kabbaj, M., Tavenas, F., and Bouchard, R. (1985). “Stress-strain-strain-rate
501 relation for the compressibility of sensitive natural clays.” *Géotechnique*, 35(2), 159-180.

502 Leoni, M., Karstunen, M., and Vermeer, P. A. (2008). “Anisotropic creep model for soft soils.”
503 *Géotechnique*, 58(3), 215-226.

504 Nash, D. F. T., Sills, G. C., and Davison, L. R. (1992). “One-dimensional consolidation
505 testing of soft clay from Bothkennar.” *Géotechnique*, 42(2), 241-256.

506 Ortiz, M. and Simo, J. C. (1986). “An analysis of a new class of integration algorithms for
507 elastoplastic constitutive relations.” *Int. J. Numer. Meth. Engng.*, 23(3), 353-366.

508 Perzyna, P. (1963). “The constitutive equations for work-hardening and rate sensitive plastic
509 materials.” *Proc. Vibr. Probl.*, Warsaw, 281-290.

510 Perzyna, P. (1966). “Fundamental problems in viscoplasticity.” *Adv. Appl. Mech.*, 9, 243-377.

511 Plaxis. (2012). PLAXIS material models manual, Delft, Netherlands.

512 Rezania, M., Taiebat, M. and Poletti, E. (2016). A viscoplastic SANICLAY model for natural
513 soft soils. Computers and Geotechnics, 73, 128-141.

514 Roscoe, K. H. and Burland, J. B. (1968). “On the generalised stress-strain behaviour of ‘wet’
515 clay.” *Engineering Plasticity*, J. Heyman and F. A. Leckie, eds., Cambridge University
516 Press, 535-609.

517 Sheahan, T. C., Ladd, C. C., and Germaine, J. T. (1996). “Rate-dependent undrained shear
518 behaviour of saturated clay.” *J. Geotech. Engrg.*, ASCE, 122(2), 99-108.

519 Sloan, S. W., Abbo, A. J., and Sheng, D. C. (2001). “Refined explicit integration of
520 elastoplastic models with automatic error control.” *Eng. Computation.*, 18(1/2), 121-194.

521 Sorensen, K. K., Baudet, B. A., and Simpson, B. (2007). “Influence of structure on the

522 time-dependent behaviour of a stiff sedimentary clay." *Géotechnique*, 57(1), 113-124.

523 Stolle, D. F. E., Vermeer, P. A., and Bonnier, P. G. (1999). "Time integration of a constitutive
524 law for soft clays." *Commun. Numer. Meth. Engng.*, 15(8), 603-609.

525 Tong, X. and Tuan, C. Y. (2007). Viscoplastic cap model for soils under high strain rate
526 loading. Journal of Geotechnical and Geoenvironmental Engineering, 133(2), 206-214.

527 Vermeer, P. A. and Neher, H. P. (1999). "A soft soil model that accounts for creep." *Proc. Int.*
528 *Symp. "Beyond 2000 in Computational Geotechnics"*, Amsterdam, 249-261.

529 Wang, L., Shen, K., and Ye, S. (2008). "Undrained shear strength of K_0 consolidated soft
530 soils." *Int. J. Geomech.*, ASCE, 8(2), 105-113.

531 Wang, L., Wang, Z., Li, L., and Wang, J. (2011). "Construction behaviour simulation of
532 hydraulic tunnel during standpipe lifting." *Tunnell. Undergr. Space Technol.*, 26(6),
533 674-685.

534 Wang, L., Dan, H., and Li, L. (2012). "Modelling strain-rate dependent behavior of
535 KR_0-consolidated soft clays." *J. Eng. Mech.*, ASCE, 138(7), 738-748.

536 Yao, Y. P., Kong, L. M., Zhou, A. N., and Yin, J. H. (2015). "Time-dependent unified
537 hardening model: three-dimensional elasto-visco-plastic constitutive model for clays." *J.*
538 *Eng. Mech.*, ASCE, 141(6), 0414162.

539 Yin, J. H., Zhu, J. G., and Graham, J. (2002). "A new elastic viscoplastic model for
540 time-dependent behaviour of normally and overconsolidated clays: theory and
541 verification." *Can. Geotech. J.*, 39(1), 157-173.

542 Yin, Z.-Y. and Hicher, P.-Y. (2008). "Identifying parameters controlling soil delayed
543 behaviour from laboratory and in situ pressuremeter testing." *Int. J. Numer. Anal. Meth.*
544 *Geomech.*, 32(12), 1515-1535.

545 Yin, Z.-Y., Chang, C. S., Karstunen, M., and Hicher, P.-Y. (2010). "An anisotropic
546 elastic-viscoplastic model for soft clays." *Int. J. Solid.s Struct.*, 47(5), 665-677.

547 Yin, Z.-Y. and Karstunen, M. (2011). "Modelling strain-rate-dependency of natural soft clays

548 combined with anisotropy and destructuration." *Acta Mech. Solida Sin.*, 24(3), 216-230.

549 Yin, Z.-Y., Zhu, Q.-Y., Yin, J.-H., and Ni, Q. (2014). "Stress relaxation coefficient and
550 formulation for soft soils." *Geotech. Lett.*, 4(1), 45-51.

551 Yin, Z.-Y., Yin, J.-H., and Huang, H.-W. (2015). "Rate-dependent and long-term yield stress
552 and strength of soft Wenzhou marine clay: experiments and modeling." *Mar. Georesour.*
553 *Geotec.*, 33(1), 79-91.

554 Yin, Z.-Y., Zhu, Q.-Y., and Zhang, D.-M. (2017). "Comparison of two creep degradation
555 modeling approaches for soft structured soils." *Acta Geotechnica.*, in press.

556

1. Tables

Table 1 State parameters and constants of elastic viscoplastic model

Type	Parameter	Definition	Determination
Modified Cam-Clay parameters	σ_{p0}^{r}	Initial reference preconsolidation pressure	From a oedometer test corresponding to a given reference strain-rate or reference time
	e_0	Initial void ratio	From a oedometer test
	υ	Poisson's ratio	From initial part of stress-strain curve
	κ	Swelling index	From oedometer test or consolidation test
	λ	Compression index	From oedometer test or isotropic consolidation test at large strain levels
	M_c	Slope of CSL in triaxial compression	From Triaxial shear test
Viscosity parameter	$C_{\alpha e}$	Secondary compression index	From 24h consolidation tests on remoulded sample

Table 2 Values of state parameters and constants of Saint-Herblain clay

Parameter	Value
σ_{p0}^{r} /kPa	39
e_0	2.26
υ	0.2
κ	0.038
λ	0.48
$M_c(M_e)$	1.2 (1.05)
$C_{\alpha e}$	0.034

Table 3 Comparison of total number of iteration and CPU time for different mesh densities by the model with different time integration methods

Algorithms	Comparison items	For mesh with element number		
		of 552	of 270	of 110
Newton-Raphson	Number of iteration	200	207	195
	CPU time (s)	70	35.1	12.1
Katona (θ=1)	Number of iteration	189	188	187
	CPU time (s)	110.1	52.8	22.7
Katona (θ=0.5)	Number of iteration	181	180	177
	CPU time (s)	84.8	51.2	22.3
Katona (θ=0)	Number of iteration	-	-	177
	CPU time (s)	-	-	17.8
Stolle et al	Number of iteration	192	188	185
	CPU time (s)	40.4	22.9	10.9
Cutting plane	Number of iteration	4803	4759	2195
	CPU time (s)	631.3	366	93.1

Table 4 Comparison of the performance of different time integration algorithms

Algorithms	1D-CRS	3D-CRS_com	3D-CRS_ext	Simple shear
Newton-Raphson	Good	Good	Good	Good
Katona (θ=1)	Good	Good	Good	Good
Katona (θ=0.5)	Fair	Fair	Fair	Good
Katona (θ=0)	Fair	Fair	Poor	--
Stolle et al	Fair	Fair	Fair	Good
Cutting plane	Fair	Fair	Fair	Good

To fill “Good” when both convergence and accuracy are good, “Fair” when one of convergence and accuracy is good, “Poor” when both convergence and accuracy are bad

Figure captions

Figure 1

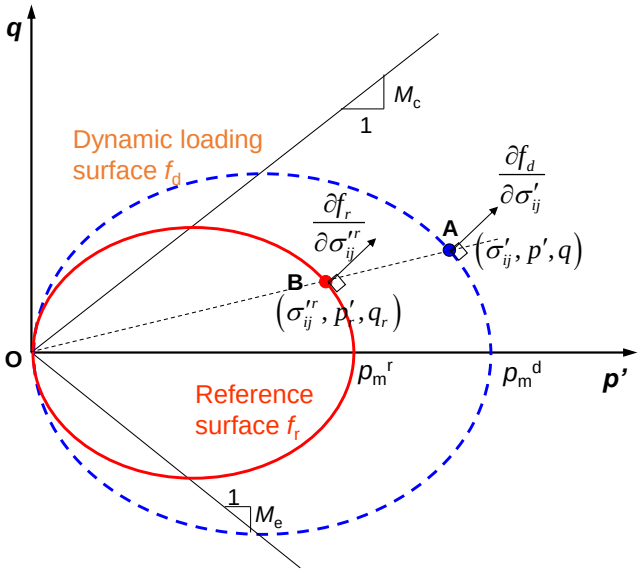
q
Dynamic loading surface f_d
M_c
1
$\frac{\partial f_d}{\partial \sigma'_{ij}}$
$\frac{\partial f_r}{\partial \sigma'^{r}_{ij}}$
A
(σ'_{ij}, p', q)
B
$(\sigma'^{r}_{ij}, p', q_r)$
O
p_m^r
p_m^d
p'
Reference surface f_r
1
M_e

Figure 2

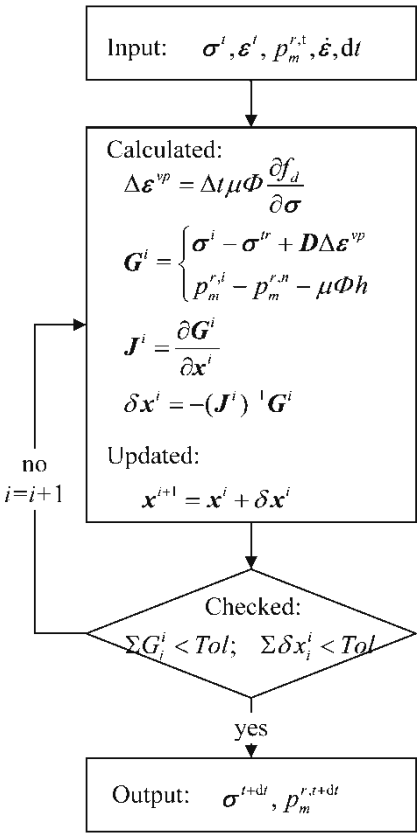
Input: $\boldsymbol{\sigma}^t, \boldsymbol{\varepsilon}^t, p_m^{r,t}, \dot{\boldsymbol{\varepsilon}}, \mathrm{d}t$
Calculated:
$\Delta\boldsymbol{\varepsilon}^{vp} = \Delta t \mu \Phi \frac{\partial f_d}{\partial \boldsymbol{\sigma}}$
$\boldsymbol{G}^i = \begin{cases} \boldsymbol{\sigma}^i - \boldsymbol{\sigma}^{tr} + \boldsymbol{D}\Delta\boldsymbol{\varepsilon}^{vp} \\ p_m^{r,i} - p_m^{r,n} - \mu\Phi h \end{cases}$
$\boldsymbol{J}^i = \frac{\partial \boldsymbol{G}^i}{\partial \boldsymbol{x}^i}$
$\delta \boldsymbol{x}^i = -(\boldsymbol{J}^i)^{-1}\boldsymbol{G}^i$
Updated:
$\boldsymbol{x}^{i+1} = \boldsymbol{x}^i + \delta \boldsymbol{x}^i$
no
$i=i+1$
Checked:
$\Sigma G_i^i < Tol; \quad \Sigma \delta x_i^i < Tol$
yes
Output: $\boldsymbol{\sigma}^{t+\mathrm{d}t}, p_m^{r,t+\mathrm{d}t}$

Figure 3

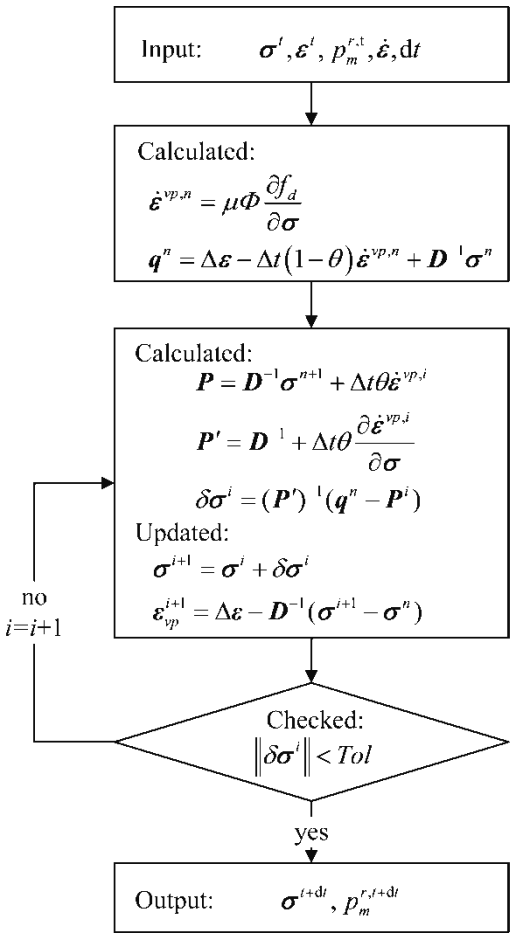
Input: $\boldsymbol{\sigma}^t, \boldsymbol{\varepsilon}^t, p_m^{r,t}, \dot{\boldsymbol{\varepsilon}}, \mathrm{d}t$
Calculated:
$\dot{\boldsymbol{\varepsilon}}^{vp,n} = \mu \Phi \frac{\partial f_d}{\partial \boldsymbol{\sigma}}$
$\boldsymbol{q}^n = \Delta\boldsymbol{\varepsilon} - \Delta t(1-\theta)\dot{\boldsymbol{\varepsilon}}^{vp,n} + \boldsymbol{D}^{-1}\boldsymbol{\sigma}^n$
Calculated:
$\boldsymbol{P} = \boldsymbol{D}^{-1}\boldsymbol{\sigma}^{n+1} + \Delta t\theta\dot{\boldsymbol{\varepsilon}}^{vp,i}$
$\boldsymbol{P}' = \boldsymbol{D}^{-1} + \Delta t\theta \frac{\partial \dot{\boldsymbol{\varepsilon}}^{vp,i}}{\partial \boldsymbol{\sigma}}$
$\delta\boldsymbol{\sigma}^i = (\boldsymbol{P}')^{-1}(\boldsymbol{q}^n - \boldsymbol{P}^i)$
Updated:
$\boldsymbol{\sigma}^{i+1} = \boldsymbol{\sigma}^i + \delta\boldsymbol{\sigma}^i$
$\boldsymbol{\varepsilon}_{vp}^{i+1} = \Delta\boldsymbol{\varepsilon} - \boldsymbol{D}^{-1}(\boldsymbol{\sigma}^{i+1} - \boldsymbol{\sigma}^n)$
no
$i=i+1$
Checked:
$\|\delta\boldsymbol{\sigma}^i\| < Tol$
yes
Output: $\boldsymbol{\sigma}^{t+\mathrm{d}t}, p_m^{r,t+\mathrm{d}t}$

Figure 4

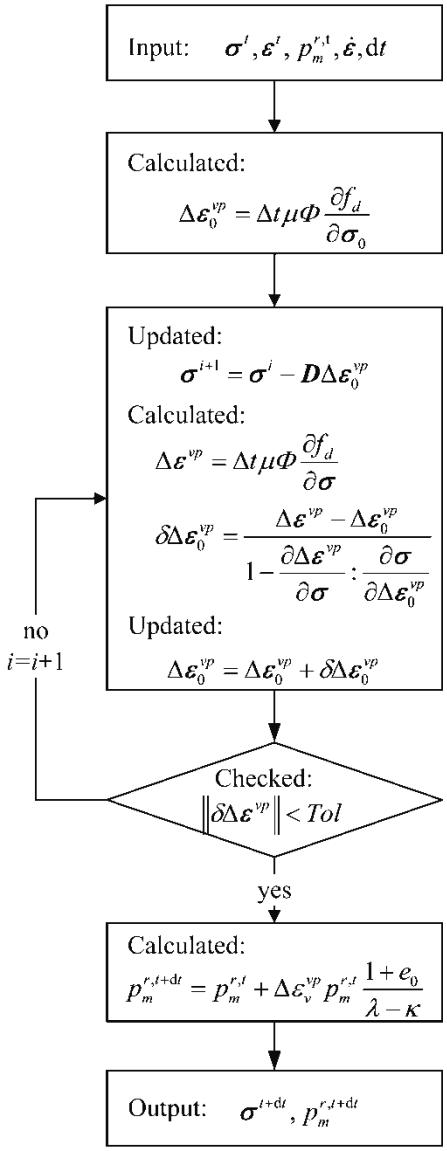
Input: $\boldsymbol{\sigma}^t, \boldsymbol{\varepsilon}^t, p_m^{r,t}, \dot{\boldsymbol{\varepsilon}}, \mathrm{d}t$
Calculated:
$\Delta\boldsymbol{\varepsilon}_0^{vp} = \Delta t \mu \Phi \frac{\partial f_d}{\partial \boldsymbol{\sigma}_0}$
Updated:
$\boldsymbol{\sigma}^{i+1} = \boldsymbol{\sigma}^i - \boldsymbol{D}\Delta\boldsymbol{\varepsilon}_0^{vp}$
Calculated:
$\Delta\boldsymbol{\varepsilon}^{vp} = \Delta t \mu \Phi \frac{\partial f_d}{\partial \boldsymbol{\sigma}}$
$\delta\Delta\boldsymbol{\varepsilon}_0^{vp} = \frac{\Delta\boldsymbol{\varepsilon}^{vp} - \Delta\boldsymbol{\varepsilon}_0^{vp}}{1 - \frac{\partial\Delta\boldsymbol{\varepsilon}^{vp}}{\partial\boldsymbol{\sigma}} : \frac{\partial\boldsymbol{\sigma}}{\partial\Delta\boldsymbol{\varepsilon}_0^{vp}}}$
Updated:
$\Delta\boldsymbol{\varepsilon}_0^{vp} = \Delta\boldsymbol{\varepsilon}_0^{vp} + \delta\Delta\boldsymbol{\varepsilon}_0^{vp}$
no
$i=i+1$
Checked:
$\|\delta\Delta\boldsymbol{\varepsilon}^{vp}\| < Tol$
yes
Calculated:
$p_m^{r,t+\mathrm{d}t} = p_m^{r,t} + \Delta\varepsilon_v^{vp} p_m^{r,t} \frac{1+e_0}{\lambda-\kappa}$
Output: $\boldsymbol{\sigma}^{t+\mathrm{d}t}, p_m^{r,t+\mathrm{d}t}$

Figure 5

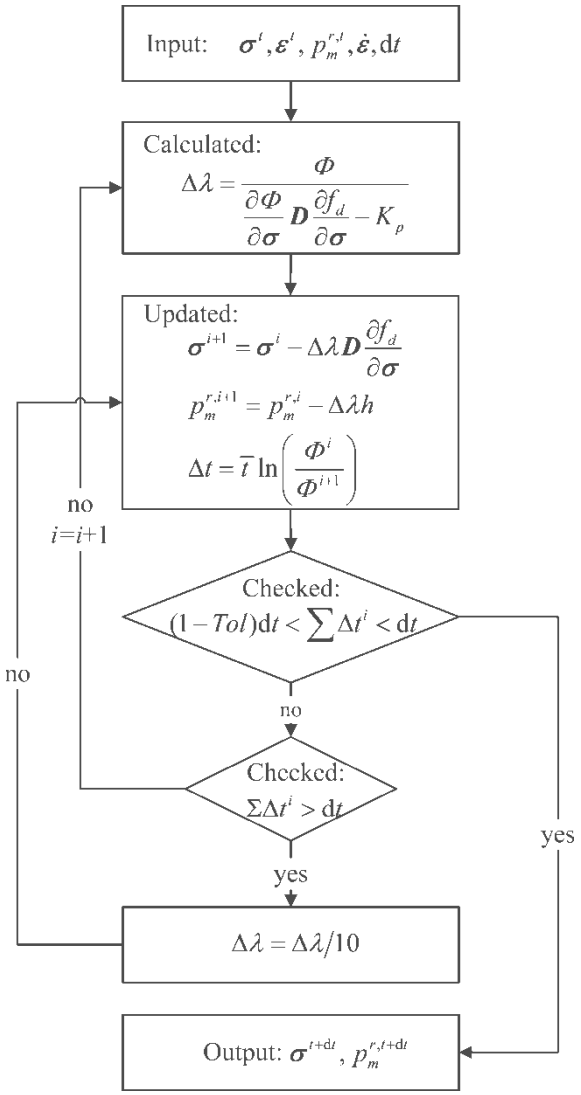
Input: $\boldsymbol{\sigma}^t, \boldsymbol{\varepsilon}^t, p_m^{r,t}, \dot{\boldsymbol{\varepsilon}}, \mathrm{d}t$
Calculated:
$\Delta\lambda = \dfrac{\Phi}{\dfrac{\partial \Phi}{\partial \boldsymbol{\sigma}} \boldsymbol{D} \dfrac{\partial f_d}{\partial \boldsymbol{\sigma}} - K_p}$
Updated:
$\boldsymbol{\sigma}^{i+1} = \boldsymbol{\sigma}^i - \Delta\lambda \boldsymbol{D} \dfrac{\partial f_d}{\partial \boldsymbol{\sigma}}$
$p_m^{r,i+1} = p_m^{r,i} - \Delta\lambda h$
$\Delta t = \bar{t} \ln\left(\dfrac{\Phi^i}{\Phi^{i+1}}\right)$
no
$i=i+1$
Checked:
$(1-Tol)\mathrm{d}t < \sum \Delta t^i < \mathrm{d}t$
no
Checked:
$\Sigma \Delta t^i > \mathrm{d}t$
yes
no
yes
$\Delta\lambda = \Delta\lambda/10$
Output: $\boldsymbol{\sigma}^{t+\mathrm{d}t}, p_m^{r,t+\mathrm{d}t}$

Figure 6

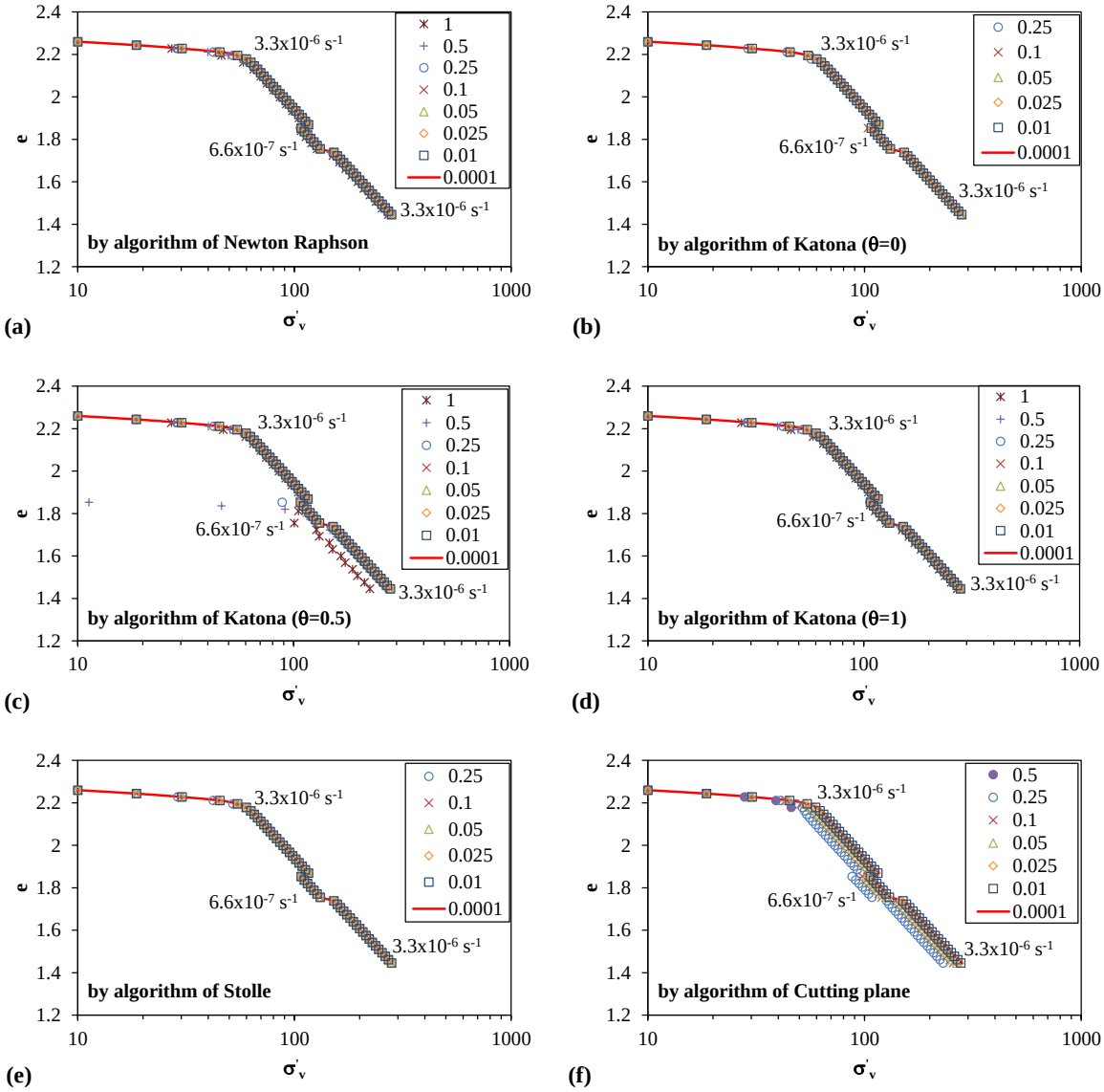
e
σ'v
3.3x10-6 s-1
6.6x10-7 s-1
1
0.5
0.25
0.1
0.05
0.025
0.01
0.0001
by algorithm of Newton Raphson
(a)
by algorithm of Katona (θ=0)
(b)
by algorithm of Katona (θ=0.5)
(c)
by algorithm of Katona (θ=1)
(d)
by algorithm of Stolle
(e)
by algorithm of Cutting plane
(f)

Figure 7

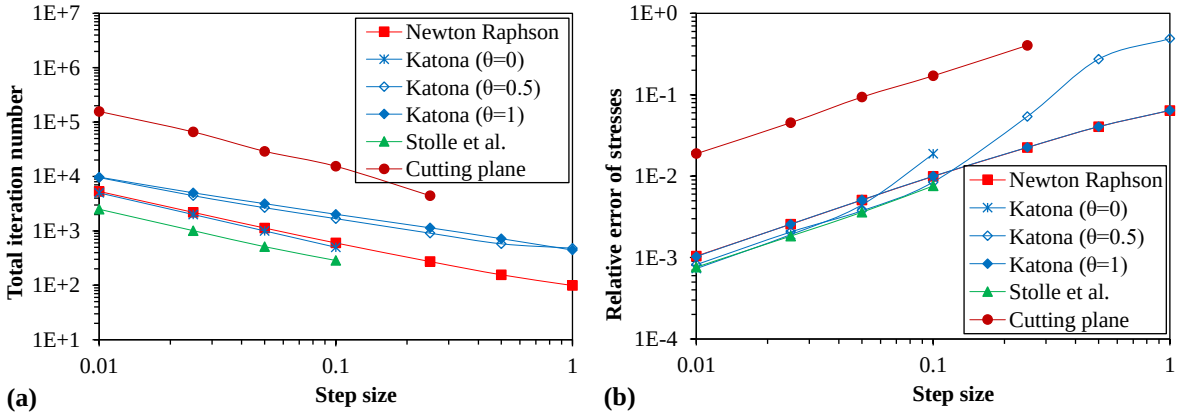
1E+7
1E+6
1E+5
1E+4
1E+3
1E+2
1E+1
Total iteration number
0.01
0.1
1
Step size
Newton Raphson
Katona (θ=0)
Katona (θ=0.5)
Katona (θ=1)
Stolle et al.
Cutting plane
(a)
1E+0
1E-1
1E-2
1E-3
1E-4
Relative error of stresses
0.01
0.1
1
Step size
Newton Raphson
Katona (θ=0)
Katona (θ=0.5)
Katona (θ=1)
Stolle et al.
Cutting plane
(b)

Figure 8

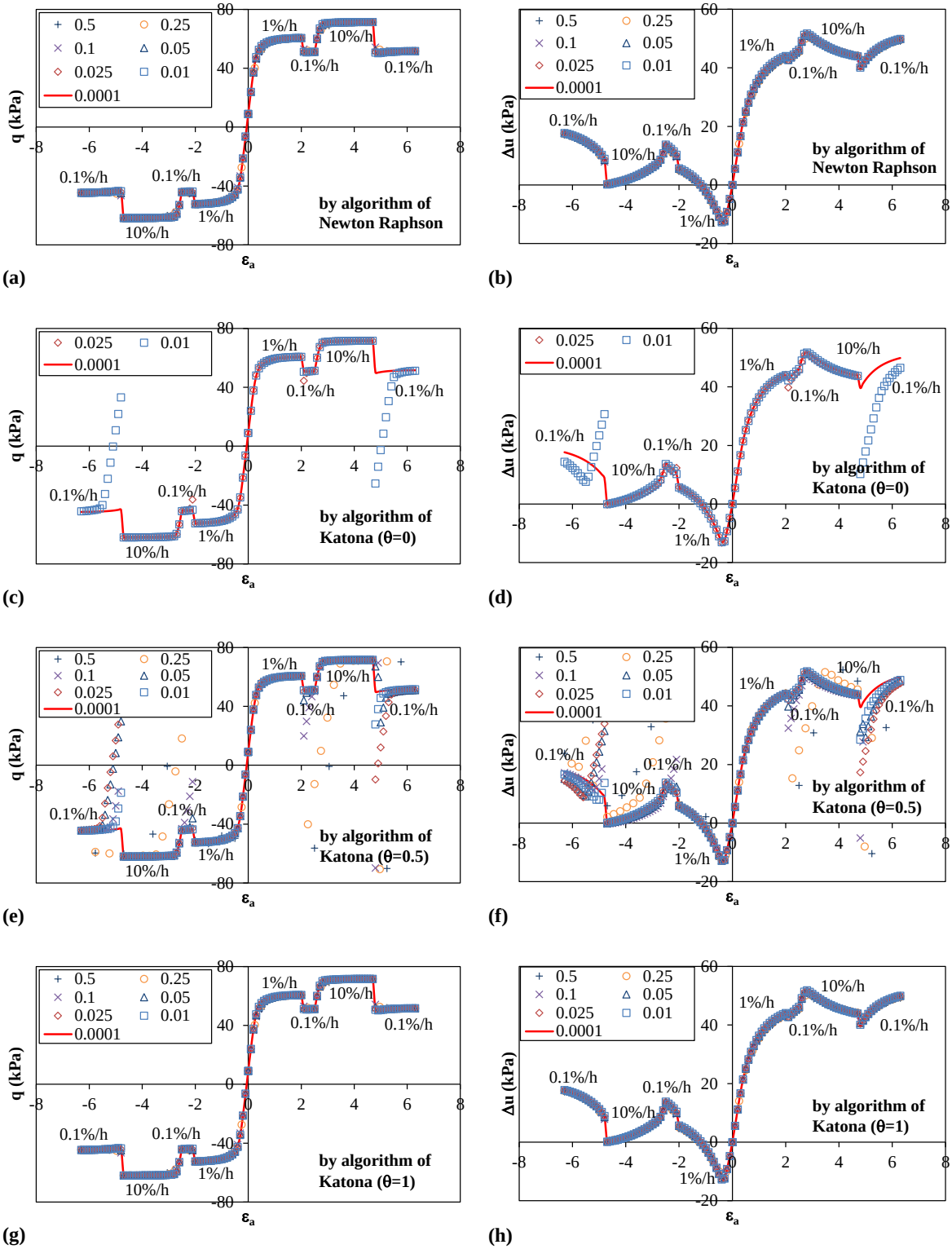
0.5
0.25
0.1
0.05
0.025
0.01
0.0001
q (kPa)
Δu (kPa)
εa
1%/h
10%/h
0.1%/h
by algorithm of Newton Raphson
by algorithm of Katona (θ=0)
by algorithm of Katona (θ=0.5)
by algorithm of Katona (θ=1)
(a)
(b)
(c)
(d)
(e)
(f)
(g)
(h)

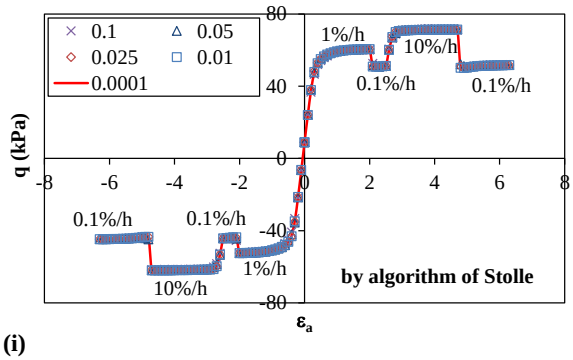
0.1
0.05
0.025
0.01
0.0001
q (kPa)
εa
1%/h
10%/h
0.1%/h
by algorithm of Stolle

(i)

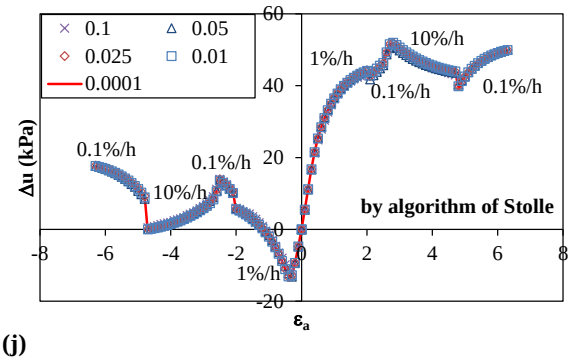
0.1
0.05
0.025
0.01
0.0001
Δu (kPa)
εa
1%/h
10%/h
0.1%/h
by algorithm of Stolle

(j)

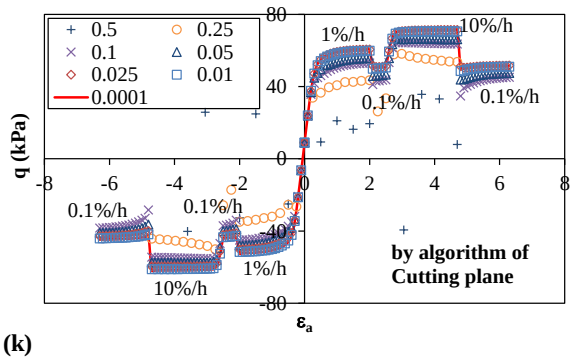
0.5
0.25
0.1
0.05
0.025
0.01
0.0001
q (kPa)
εa
1%/h
10%/h
0.1%/h
by algorithm of
Cutting plane

(k)

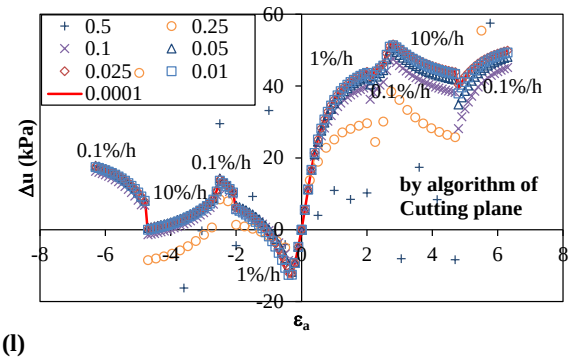
0.5
0.25
0.1
0.05
0.025
0.01
0.0001
Δu (kPa)
εa
1%/h
10%/h
0.1%/h
by algorithm of
Cutting plane

(l)

Figure 9

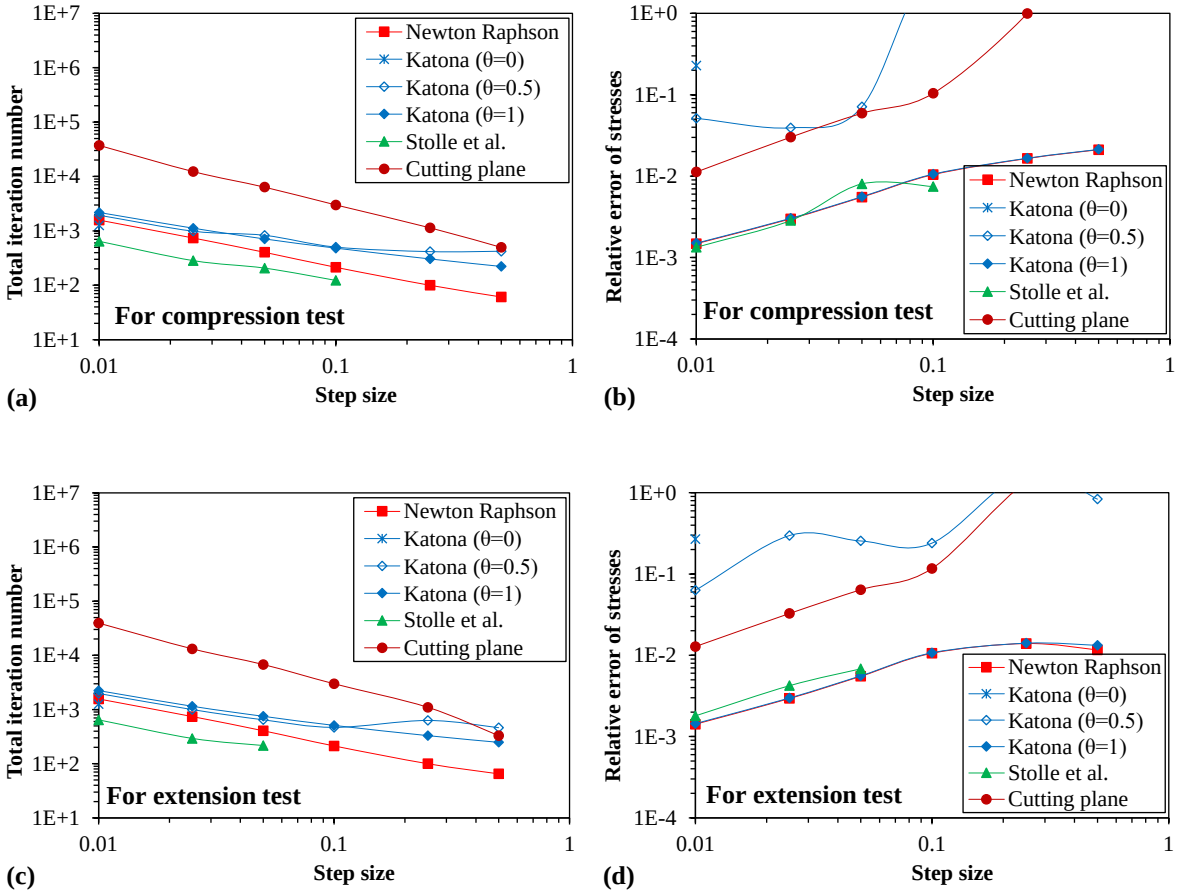
Total iteration number
Step size
Relative error of stresses
Newton Raphson
Katona (θ=0)
Katona (θ=0.5)
Katona (θ=1)
Stolle et al.
Cutting plane
For compression test
For extension test
(a)
(b)
(c)
(d)

Figure 10

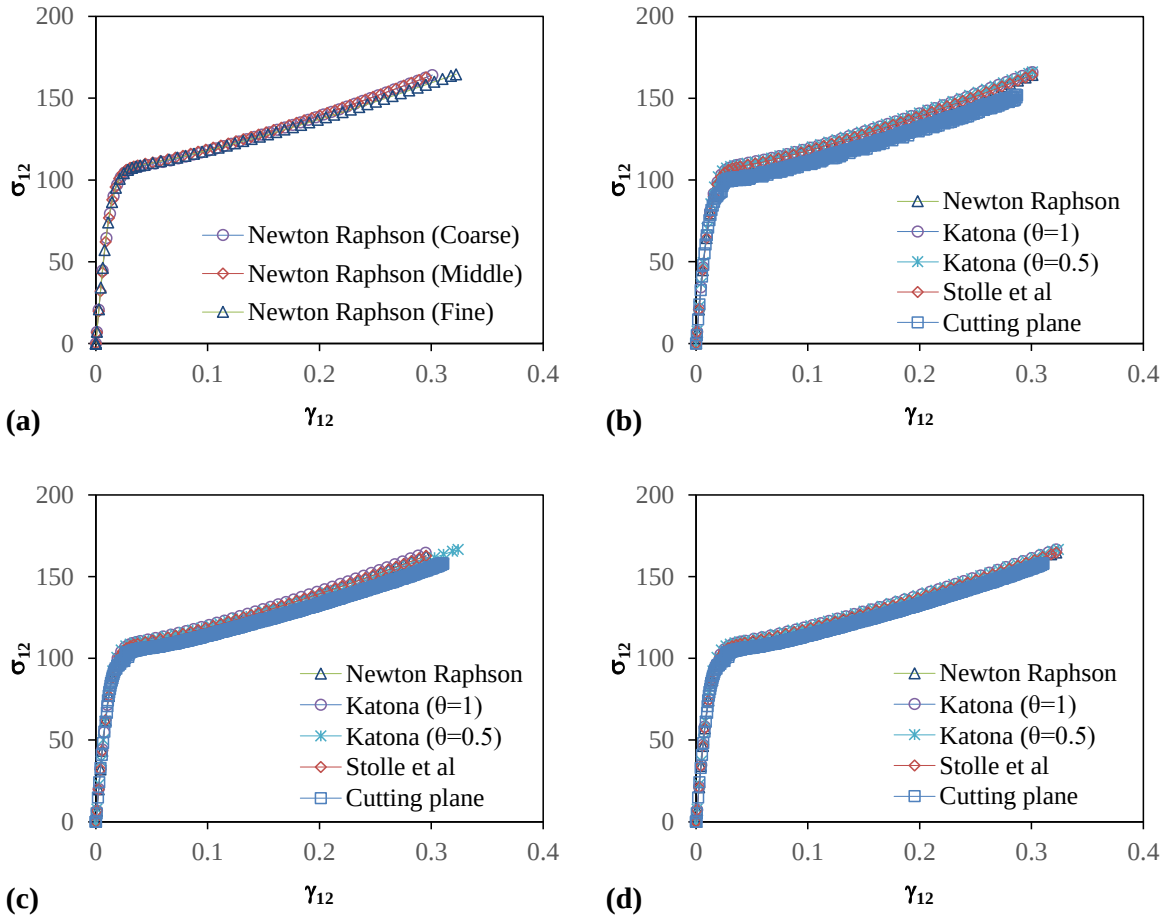
200
150
100
50
0
σ12
0
0.1
0.2
0.3
0.4
γ12
Newton Raphson (Coarse)
Newton Raphson (Middle)
Newton Raphson (Fine)
(a)
Newton Raphson
Katona (θ=1)
Katona (θ=0.5)
Stolle et al
Cutting plane
(b)
(c)
(d)

Figure 11

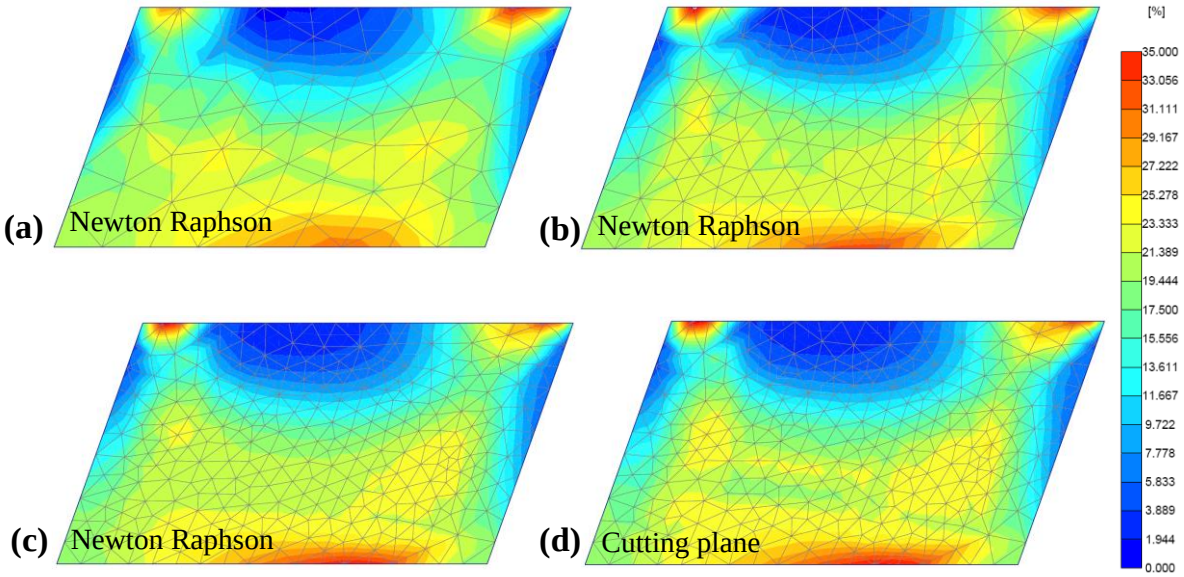
(a) Newton Raphson
(b) Newton Raphson
(c) Newton Raphson
(d) Cutting plane
[%]
35.000
33.056
31.111
29.167
27.222
25.278
23.333
21.389
19.444
17.500
15.556
13.611
11.667
9.722
7.778
5.833
3.889
1.944
0.000